ChemPubSoc Europe

DOI: 10.1002/batt.201900113

BATTERIES & SUPERCAPS
Articles

Versatile Synthesis of Vanadium(III, IV, V) Oxides@Reduced Graphene Oxide Nanocomposites and Evaluation of their Lithium and Sodium Storage Performances

Xuelian Liu,[a] Sébastien Depaifve,[b] Tom Leyssens,[a] Sophie Hermans,[a] and Alexandru Vlad*[a]

Vanadium oxides (VO_x) have been extensively investigated over the past years as promising electrode materials for alkali ion batteries owing to their rich and interesting electrochemical properties. Further improvements on electrochemistry of VO_x materials have been possible by working at the nanoscale as well as by realising hierarchical composites with various carbon allotropes. However, the nanocomposite synthesis methods are not always efficient, nor green, requiring either expensive precursors, extended synthesis time or harmful reagents. Herein, we report on rapid and environmentally friendly synthesis methods of a library of VO_x@rGO composites via impregnation and hydrothermal protocols using a cheap and commercially available V_2O_5 precursor. Different oxidation states, crystalline phases and nanoscale morphologies can be reproducibly accessed and their physico-chemical properties have been characterized. The electrochemical properties (lithium and sodium ion storage) of the synthesized VO_x@rGO nanocomposites and phases have been critically inter-compared between these but also with respect to commercial (CM) VO_x-based electrodes. Whereas nanostructuring is found to impact the power-rate performances, the amount of stored charge and the cycling stability are sensitively dependent on the cycling potential window, while being minorly affected by the morphology and synthesis method. The composites are also found to exhibit different electrochemistry for sodium storage, with more sloping potential profiles. Peculiarly, the synthesized V_2O_3@rGO composite shows no signs of electrochemical activity pointing towards the electrochemical inertness of this particular V_2O_3 composite and phase. This work could serve as reference for future developments on this class of important battery materials as it is one of the few studies describing a comprehensive and comparative study of several different influential parameters on the electrochemical behaviour of vanadium oxides in different oxidation states, crystalline phases and morphologies.

1. Introduction

With their structural flexibility and interesting chemical and physical properties, vanadium oxides have been widely utilized in many fields such as catalysis,[1] chemical sensors[2] and energy storage.[3] When applied as electrode materials for lithium-ion batteries (LIBs), one of the most successfully commercialized energy storage systems, vanadium oxides have been shown to exhibit rich electrochemistry due to the availability of different oxidation states and phase structures.[4] Besides, vanadium is more abundant than cobalt in Earth's crust, and therefore Vanadium-based chemistries could be an interesting and lower-cost alternative over the conventional Cobalt-based chemistries, which makes them further attractive for researchers in the energy storage community.[5]

When analysing the progress in the field of vanadium oxides battery materials, a series of main aspects appear as most important to understand but also enable efficient energy storage with vanadium oxides as electrode material, namely:

i) nanostructuring, with the addition of carbon nanomaterials to form composites has a crucial effect on electrochemical performance and in particular on power-rate capability.
ii) phase structure and composition affects the electrochemical properties, and in particular the potential profile and the attained charge storage capacities; despite, the redox potential cycling window seemingly affects the first cycle efficiency but also the overall capacity retention with cycling, an aspect that still remains poorly explored thus far.
iii) whereas many V_2O_3 phases are reported to be electrochemically active, herein we find one particular phase and nanoscale morphology that shows no electrochemical activity, requiring further in depth studies to understand the origin of this peculiar behaviour. Additionally, the lowest attained valence for electrochemical lithiation of vanadium oxide - based compounds found in literature is around III.

[a] X. Liu, Prof. T. Leyssens, Prof. S. Hermans, Prof. A. Vlad
Institute of Condensed Matter and Nanosciences (IMCN)
Université Catholique de Louvain
Louvain-la-Neuve, 1348 (Belgium)
E-mail: alexandru.vlad@uclouvain.be
[b] S. Depaifve
Luxembourg Institute of Science and Technology (LIST)
Materials Research and Technology Department (MRT)
5 rue Bommel, ZAE Robert Steichen, Hautcharage, 4940 (Luxembourg)

Supporting information for this article is available on the WWW under https://doi.org/10.1002/batt.201900113

This publication is part of a joint Special Issue with ChemSusChem focusing on "2D Energy Storage Materials"

iv) finally, most of the reports to date deal with the electrochemical performance enhancement using methods in (i) and (ii), yet limited to only one (and rarely few) vanadium oxide composition (valence state), nanoscale morphology or phase in a one single study. A clear comparison between the impact of these is difficult since also different procedures for cell assembly and testing are being used. Altogether, these points require a comparative analysis of vanadium oxides electrochemistry in order to select the most performing candidates.

Further detailing the criterion (i), it should be noted thatVO_x have intrinsic poor electrical conductivity and slow cation de/insertion kinetics.[4b,5b,6] Consequently, two main strategies have been extensively applied to overcome these drawbacks and attain full material utilisation at also high current densities. Nanostructuring has been regarded as one of the most effective strategies to improve electrochemical performance of electrode materials. The nanostructured morphology not only shortens Li-ion and electron transport distances in electrodes, but also enables active materials and composite electrodes to sustain volume changes and stresses during cycling, resulting in improved rate capability and stability of the active material as well as of the electrode construct.[7] The second strategy relates to hybridizing carbon allotropes with nanoscale VO_x. In particular, graphene as a novel carbon material has been extensively used for producing composite electrode materials with improved Li storage performance, benefiting from the well-defined nanostructure, high specific surface area and high electrical conductivity.[8] For example, graphene nanoribbon-V_2O_5,[9] VO_2(B)/rGO composite[10] and V_2O_3/rGO composite[11] have been shown to considerably improve the electrochemical properties, compared to equivalent material morphology and composition materials yet without conductive graphene support. However, the large discrepancies still present in graphene materials composition, morphology and physico-chemical properties leads to composites being synthesized and tested under different conditions, making difficult the comparison and discrimination of the electrochemical performance metrics of the respective phases.

Concerning the criterion (ii), V_2O_5 being the most stable phase among all vanadium oxides, remains the most studied for electrochemical applications, with complex mechanisms associated with Li^+ de/intercalation still remaining to elucidate. Various phase transitions have been revealed in the discharge profile through defined potential steps at around 3.4, 3.2 and 2.3 V (*vs.* Li^+/Li) corresponding to the α/ε, ε/δ, and δ/γ two-phase regions, respectively.[5b,12] The theoretical capacity is of 294 mAh g^{-1} (accounting also for the inserted Li cations), for a two Li^+-two electron reaction per formula unit (corresponding to $Li_2V_2O_5$). It has been reported that further intercalation of Li into V_2O_5 would lead to irreversible formation of ω-$Li_xV_2O_5$ ($2 < x < 3$).[13]

Chan *et al.* reported chemical lithiation of V_2O_5 nanoribbons with subsequent delithiation of ω-$Li_3V_2O_5$ back to the pristine V_2O_5 nanoribbon, attributed to its ability of facile strain relaxation and phase transformation at nanoscale.[14] Concurrent to this, it has been reported recently that the deep lithiated ω-$Li_3V_2O_5$ phase can be reversibly transformed into disordered β-$Li_{0.3}V_2O_5$ phase via a two-phase reaction.[15] Both disordered structures show good stability, indicating the potential of disordered phases as electrode materials. Recently, electrochemical performance of amorphous V_2O_5 thin films (prepared by atomic layer deposition method) has been also investigated and compared to that of their crystalline counterpart.[16] The amorphous V_2O_5 electrode was found to have cyclic voltammogram profiles without sharply defined peaks displayed by crystalline V_2O_5. Despite, these work detailed only on Li-cation insertion with also the working potential window not being optimized leading to major irreversible first cycle losses, with further cycling not being representative of pristine crystalline or amorphous phases.

When looking at vanadium oxides in lower oxidation states, VO_2 is known to exist in several polymorphs, among which the metastable VO_2(B) with a monoclinic structure is the most studied for charge storage applications.[17] VO_2(B) displays redox potential plateaus at 2.5–2.6 V (*vs.* Li^+/Li), high specific capacity and good stability as cathode material.[18] The electrochemical properties of amorphous VO_2 were also reported recently and the authors found it to store more charge and at higher current densities than VO_2(B).[16b] However, the attained capacities of the amorphous electrode were already higher than expected, pointing towards other than faradaic processes at play, presumably originating from particular micro-electrode design with high surface area or possible phase impurities.

Going further down, V_2O_3 has been also extensively studied, yet the discrepancies here are even more pronounced between different studies as well as compared to theoretical predictions. For instance, Hong *et al.* studied the Li uptake into, and extraction from various metal oxides, including VO_x. The calculated capacity of V_2O_3 was 1073 mAh g^{-1}. However, the full Li uptake and reduction of V_2O_3 to metallic V^0 was not realized or seemed to be difficult to attain.[19] After a detailed analysis performed by us, we found that the reported capacity values of V_2O_3 electrode (most of the time cycled to low potentials) differ significantly, depending on structure, morphology and modification with carbon calling for better understanding of the electrochemistry of this material. Additionally, analysis of literature of V_2O_5 and VO_2 also points to the fact that electrochemical reduction of V^{3+} is hard to realize when in an oxide matrix.

And finally, regarding the criterion (iv), clearly vanadium oxides have attracted and continue to attract interest as electrode materials for lithium but also recently for sodium, potassium and divalent cation storage.[20] High storage capacity, suitable working potential as well as power performances make VO_x potential candidates for energy storage. Yet, it is scarce that more than one vanadium oxides (phase, valence)-carbon composites are prepared under similar conditions and their electrochemical properties are measured, compared and discussed systematically in a single publication. This makes a critical comparison and choice of the best material difficult.

In this work, we controllably synthesize a library of VO_x@rGO composites with different vanadium oxidation states, morphologies and phases via similar methods and with similar

carbon content and morphology. Stable and cheap V_2O_5 was selected as vanadium source, exploiting its solubility and reduction ability in acidic aqueous solutions, rendering this process easily available to others. Moreover, commercial rGO was employed as structural and electrical conduction framework.

The simple synthetic strategy allows us to conduct a systematic comparison study of the electrochemical properties for different vanadium oxide phases. Li and Na cells have been built and tested using similar cell configuration, electrolyte and mass loadings. The potential profile characteristics during the insertion/extraction of Li^+/Na^+ as well as first cycle efficiency and cycling stability were evaluated in various potential windows, and their rate capabilities are also reported.

2. Results and Discussion

Many methods have been proposed to synthesize nanostructured vanadium oxides including sol-gel, reverse micelle templating, electrochemical deposition and solvo/hydrothermal synthesis.[21] Among them, hydrothermal synthesis is considered the easiest and most effective way to achieve nanostructured vanadium oxides deposits on the surface of nanocarbons. However, it is still challenging to achieve a facile, cost-effective and environmentally friendly synthesis to produce VO_x/C materials with well-defined structures, pure and crystalline phases (for a detailed discussion refer to Note S1 in the Supporting Online document).

The synthesis methods of the VO_x@rGO library, as displayed in Scheme 1, rely on the use of cost-effective V_2O_5 as starting material, commercial rGO as support, without addition of surfactant or other additives and environmentally friendly acids (oxalic and citric acids) as reducing and capping agents (Figure S1). A library of vanadium oxides nanostructures (Figures 1 and S2) were easily obtained using this versatile and green approach and directly deposited on rGO sheets in one pot (for a detailed discussion refer to Note S1 in the Supporting Online document).

Figure 1 groups the phases and morphologies of the synthesized VO_x@rGO composites. For comparative purposes, the XRD patterns of commercial (CM) VO_x samples are also given, whereas SEM images of the respective samples are shown in Figure S3. Starting rGO shows a broad diffraction peak with the diffraction peaks associated to graphite absent, indicating that the used rGO is well exfoliated.[22] As depicted in Figure 1, all the synthesized composites display the broad peak of rGO as well as a series of minor peaks matching to the diffraction peaks of commercial analogues. From these we can deduce that the synthesized as well as commercial phases used are as follows: V_2O_5@rGO and V_2O_5(CM)-orthorhombic; VO_2(B)@rGO, VO_2(CM) and VO_2(M/B)@rGO-monoclinic; and V_2O_3@rGO and V_2O_3(CM)-rhombohedral. For the VO_2(AM)@rGO, no additional peaks could be assigned, confirming its amorphous phase. The carbon content was analysed by thermogravimetric analysis and all composites have been found to contain similar amount of rGO (Figure S4, Table S1).

Figure 1 also illustrates the nanoscale morphology of the synthesized VO_x@rGO composites with typical VO_x particles size below 1 μm, with also uniform dispersion of VO_x nanoparticles within the rGO matrix (Figure S5). The composites present different VO_x morphologies with typically: nanoparticle for V_2O_5, cuboidal for VO_2(B) and urchin-like for the others. The CM materials have a typical particle size of over 1 μm (Figure S3).

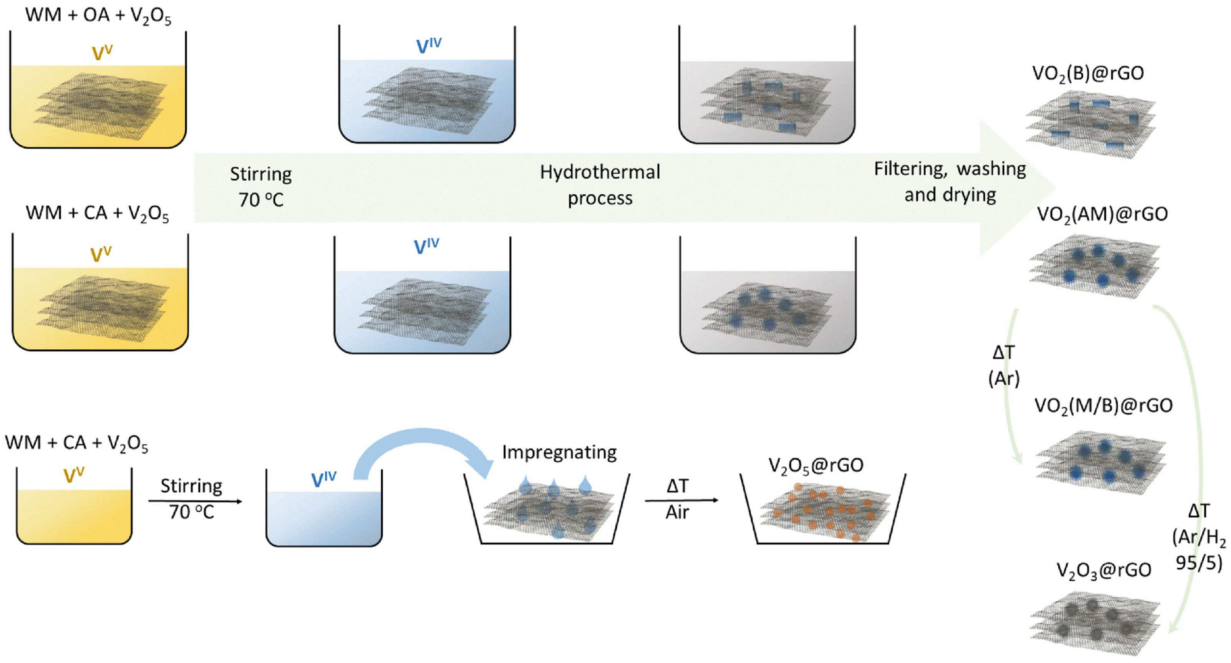

Scheme 1. Summary of the VO_x@rGO library synthesis methods developed in this work. WM=Water/MeOH = 7/1 (v/v) mixture; CA = citric acid; OA = oxalic acid.

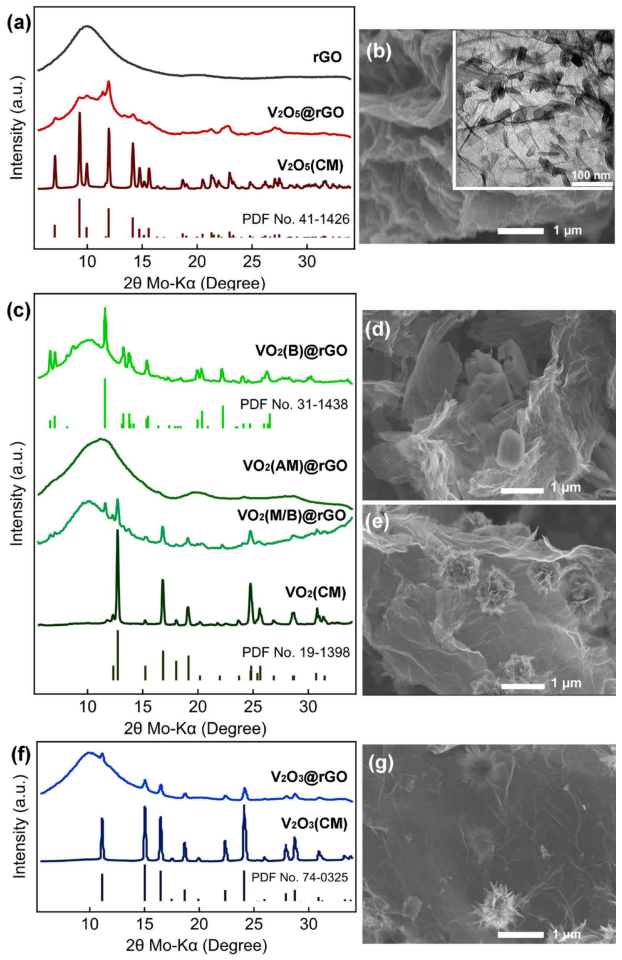

Figure 1. XRD patterns of (a) rGO, V_2O_5@rGO and V_2O_5(CM), (c) VO_2@rGO nanocomposites and VO_2(CM) and (f) V_2O_3@rGO and V_2O_3(CM). SEM images of (b) V_2O_5@rGO with an inset of TEM image, (d) VO_2(B)@rGO, (e) VO_2(AM) @rGO and (g) V_2O_3@rGO.

The synthesized VO_x@rGO composites have thus lower characteristic dimensions with also more uniform particle size distribution expected to positively impact the power-rate performances as detailed next.

With the morphology and the composition being established, we next entailed electrochemical performance analysis for Li^+ as well as Na^+ storage. The main property we screened was the optimal operation potential window to enable high capacity charge storage while not compromising the cycling stability and coulombic efficiency.

First thing to notice here is that the V_2O_5@rGO electrodes exhibit sloping potentials *vs.* capacity charge-discharge profiles, with indistinct plateaus even during the initial cycling (Figures 2a,b,c), different from those of V_2O_5(CM) (Figure 2d) but similar to those of amorphous V_2O_5 found in literatures.[16b,23] In general, electrode materials with crystalline phase display plateaus in the charge-discharge potential profiles because of abrupt phase changes at certain amount of de/intercalated Li^+, whereas amorphous electrodes typically have sloping potential curves due to lack of evident phase transformations during insertion / extraction of Li^+.[16b,23] XRD pattern of the synthesized V_2O_5@rGO (Figure 1a) also confirms that the material has poor crystallinity, being probably a mixture of crystalline and amorphous phases. Furthermore, as shown by the TEM analysis, the particles are less than 100 nm in size with similar to flakes morphology. The material is thus characterized by surface rather than bulk redox, explaining the potential profiles similar to those of amorphous electrode materials.

Next, we targeted the cycling stability and coulombic efficiency function of the cycling potential window (Figures 2e, f). Within the working potential window of 1.0–4.1 V (*vs.* Li^+/Li) high initial capacities, of up to 500 mAh g^{-1}_{V2O5} (per gram of V_2O_5 in the composite) are attained. This would correspond to 3.4 Li^+ insertion and extraction per formula unit, exceeding the typical 3 Li^+ insertion (ω-$Li_3V_2O_5$). This has also been observed by others and could be explained by additional capacitive contribution by the high surface area electrodes (summed up contribution rGO and V_2O_5).[24] The capacitive storage contribution of rGO was thus tested (Figure S6). Within the cycling window of 1.0–4.1 V (*vs.* Li^+/Li), the rGO can store almost 55 mAh g^{-1}_{rGO}, corresponding to capacity contribution of 15 mAh g^{-1} to V_2O_5@rGO (based on the calculation considering rGO content in the composite), which still does not suffice to balance the extra capacity. This could mean that the additional part of the attained capacity in V_2O_5@rGO could come from the V_2O_5 high surface material synthesized in this work or the onset of irreversible electrolyte decomposition at low potentials.

To further evidence the influence of deep lithiation limit on the reversibility and stability of V_2O_5@rGO, a galvanostatic charge-discharge test was performed with a gradually extending potential window: from 3.6–2.0 to 3.6–1.0 V (*vs.* Li^+/Li). As the results show in Figure 2f, the capacity indeed increases while extending potential window at the sacrifice of lower cycling stability. This could be already noticed by a decline in CE of close to 100% in the limited potential window to less than 90% when cycling in the extended potential window. This evidences that deep insertion of Li^+ can worsen the reversibility of the electrode, which could be due to the formation of irreversible phase (ω-$Li_3V_2O_5$), dissolution of V in electrolyte under deep discharge conditions, as well as electrolyte decomposition.[12,25]

Whereas appealing charge storage metrics can be attained in this extended potential window (3.6–1.0 V *vs.* Li^+/Li), major irreversible changes are observed in the following cycles, with severe capacity loss and an average coulombic efficiency below 90% (Figures 2e,f). This is further significant of irreversible ω-phase changes during deep lithiation of V_2O_5, as also described in literature.[16,17] When limiting the potential window to 2.0–3.6 V (*vs.* Li^+/Li), the first cycle discharge capacity decreases to 269 mAh g^{-1}_{V2O5}, equivalent to 1.8 Li^+ insertion per formula unit (corresponding to $Li_{1.8}V_2O_5$). The cycling becomes highly reversible, with considerably improved capacity retention and an average coulombic efficiency of 100% (Figure 2e). When extending the working potential window to higher values, the gain in the amount of stored charge is minimal, whereas the stability is again reduced. For example, if the upper potential is raised to 4.6 V (*vs.* Li^+/Li), similar capacities yet with faster degradation are obtained as compared to stable cycling

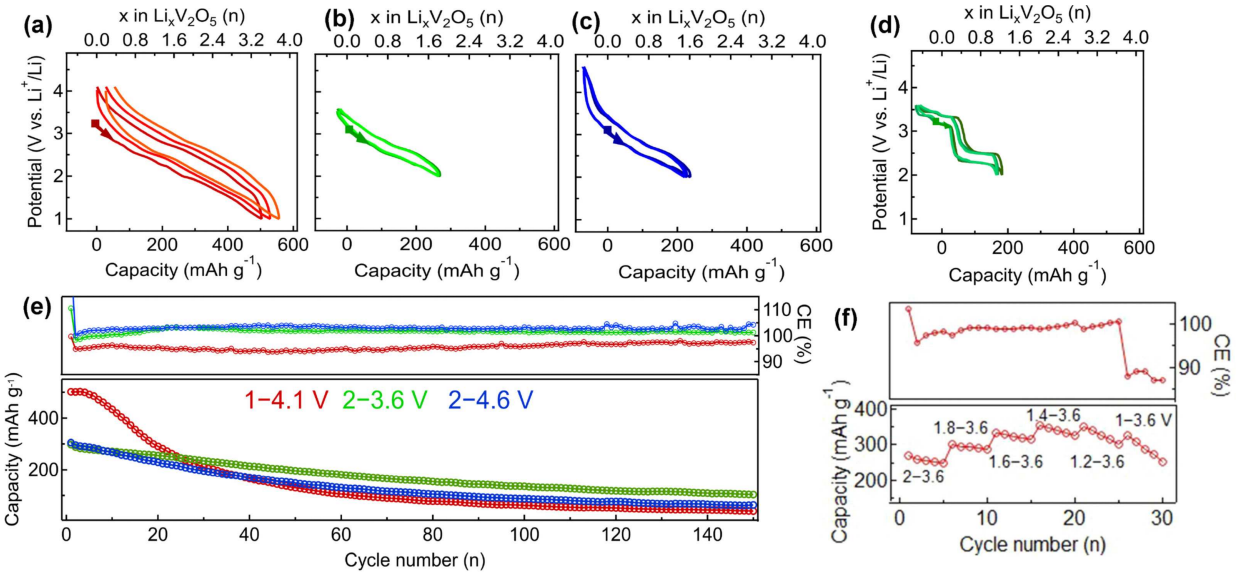

Figure 2. Galvanostatic potential versus gravimetric capacity (bottom axis) and Li-content (top axis) profiles for V_2O_5@rGO electrodes cycled in potential window of (a) 1.0–4.1 V, (b) 2.0–3.6 V; (c) 2.0–4.6 V; and (d) comparison with for V_2O_5(CM) electrode in the 2.0–3.6 V window. (e) Charge capacity and coulombic efficiency (CE) retention with cycling, at constant charge–discharge current density of 100 mA $g^{-1}_{(V2O5)}$. (f) Coulombic efficiency and stored charge amount chart in various potential windows at charge-discharge current density of 30 mA $g^{-1}_{(V2O5)}$.

window (2.0–3.6 V *vs.* Li^+/Li). This could be explained by increased electrolyte decomposition at the rGO or V_2O_5 surfaces.

Our results on V_2O_5@rGO are consistent with comparative and statistical analysis of nearly a hundred V_2O_5 electrodes in a recent review article.[26] Limiting lithiation at 2 Li^+ (corresponding to $Li_2V_2O_5$, equivalent to 294 mAh g^{-1}) could be favourable for V_2O_5 electrode to deliver decent capacity with good cycling stability. Moreover, the controllable synthesis method and similar test conditions for the electrodes make comparisons reliable and straightforward. Additionally, we take capacitive effects into consideration when the electrochemical performances of the nanoscale V_2O_5 are evaluated.

Similar methodology was applied to VO_2 (B) and (AM) phases and they show some similarities in capacity value and cycling trends, as summarized in Figure 3. When tested in the window of 1.0–4.1 V (*vs.* Li^+/Li), the electrodes delivered initial capacities of approximately 400 mAh g^{-1}_{VO2} with reversible capacities of around 300 mAh g^{-1}_{VO2}. This is nearly the theoretical value (323 mAh g^{-1}), corresponding to 1 Li^+ transfer per formula unit. The irreversible part could be ascribed to the side-reaction between the electrode and electrolyte at first cycle.[27] With fluctuations during the first 40 cycles, the capacity decreased drastically in the following cycles. Gradual capacity losses are also detected when the working potential window is extended to 2.0–4.6 V (*vs.* Li^+/Li), resulting from decomposition

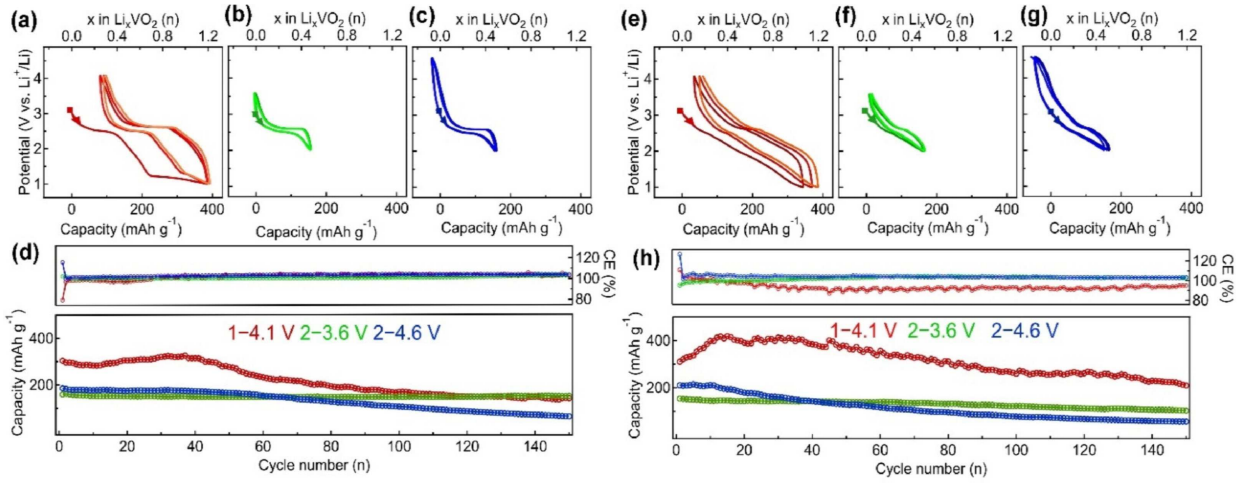

Figure 3. Galvanostatic charge-discharge tests at 100 mA $g^{-1}_{(VO2)}$. Potential *vs.* specific capacity and Li content profiles in potential window of (a) 1.0–4.1 V, (b) 2.0–3.6 V and (c) 2.0–4.6 V and (d) charge capacity and CE *vs.* cycle number, cycling performance for VO_2(B)@rGO, and the profiles in the window of (e) 1.0–4.1 V, (f) 2.0–3.6 V and (g) 2.0–4.6 V and (h) the cycling performance for VO_2(AM)@rGO.

of electrolyte. Only the electrode measured in the potential window of 2.0–3.6 V (*vs.* Li^+/Li) displayed excellent cycling stability and CE, with high capacity retention (over 150 cycles) of 96% and 67% for VO_2(B)@rGO and VO_2(AM)@rGO, respectively.

Whereas the cycling stability function of redox potential window dependence seems to be similar between both, VO_2(B)@rGO and VO_2(AM)@rGO electrodes, different potential profiles function of composition are obtained. The good crystallinity of the synthesized VO_2(B)@rGO results in clearly defined Li^+ insertion and extraction plateau at around 2.6 V (*vs.* Li^+/Li), in agreement with previous reports.[10,18b] In contrast, the VO_2(AM)@rGO electrode potential profile mainly shows sloping features, consistent with the amorphous nature of the electrode, namely no distinctive transformation of crystalline structures during Li^+ insertion/extraction.[16b,28] The disordered framework of the amorphous materials can facilitate ionic diffusion and charge storage, which could explain why VO_2(AM)@rGO delivers an average charge storage capacity of 317 mAh g^{-1}_{VO2} (almost 1 Li^+ extraction) in the wide window of 1.0–4.1 V (vs. Li^+/Li).[29]

To further get insight into the electrochemical behaviour differences between the VO_2(B)@rGO and VO_2(AM)@rGO, the electrodes were galvanostatically cycled at low current density of 10 mA g^{-1} in the stable cycling potential window (of 2.0–3.6 V *vs.* Li^+/Li). The potential vs. specific capacity and dQ/dV *vs.* V profiles are shown in Figure 4. As also pointed above,

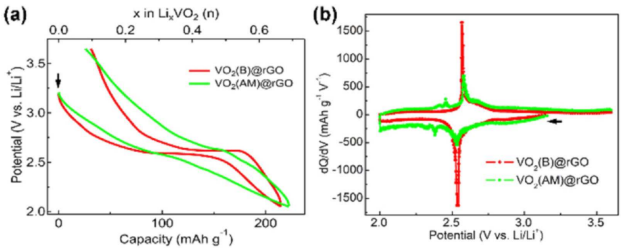

Figure 4. Comparison of galvanostatic charge-discharge performance at 10 mA $g^{-1}_{(VO2)}$ at the first cycle for VO_2(B)@rGO and VO_2(AM)@rGO. (a) Potential *vs.* specific capacity and (b) dQ/dV *vs.* V profiles.

both electrodes were found to exhibit similar capacity (220 mAh g^{-1}_{VO2} corresponding to 0.7 Li^+ transfer) and first cycle reversibility (86%). Yet, only VO_2(B)@rGO displays a noticeable reduction and oxidation plateau around 2.6 V (vs. Li^+/Li). This is also evidenced by the intense pair of peaks in the corresponding dQ/dV *vs.* V profile, due to the phase transition of VO_2(B) during Li^+ insertion and extraction.[18b]

The additional peaks in the dQ/dV *vs.* V profile for VO_2(AM)@rGO electrode are consistent with the literature and are characteristic of redox processes of low-valent vanadium oxides during Li^+ insertion into and extraction from VO_2(AM).[30] The dQ/dV profiles of all tested phases, including also VO_2(M/B)@rGO and VO_2(CM) are summarized in Figure S7. The M-phase VO_2(CM) electrode shows poor Li^+ insertion and extraction with also low capacities attained, which suggests poor electrochemical activity, as it is also the case for VO_2(M/B)@rGO. Prepared through post thermal treatment of VO_2(AM)@rGO, VO_2(M/B)@rGO has inherited the morphology but becomes crystalline with both M phase and B phase present. It can be thus stated that the amorphous and B-phase VO_2 are more suitable as electrode materials for LIBs, compared to their M-phase counterpart.

To summarize, when cut-off potential limits down to 1 V, all the V_2O_5@rGO and VO_2@rGO electrodes suffer from poor cycling stability, with ca. 3.4 and 1 Li^+ insertion per formula unit at first discharge, respectively. The lowest attainable valence of vanadium is thus roughly V^{3+}. Deep Li^+ insertion into V_2O_5 and VO_2 is also found to lead to irreversible or unstable phases. Additionally, there might exist barriers to further electrochemical reduction of vanadium to the lower valence. On the contrary, the electrodes show enhanced cycling performance in the narrow window of 2.0–3.6 V (*vs.* Li^+/Li), with less Li^+ insertion, of *ca.* 1.8 and 0.5 Li^+ for V_2O_5@rGO and VO_2@rGO, respectively. Whereas it has been already reported that insertion of more than 2 Li^+ into V_2O_5 could form irreversible phases (ω-$Li_xV_2O_5$), phase reversibility of deep Li^+ insertion into VO_2 remains scarcely studied.

Finally, we also analysed and report here the electrochemistry of the V_2O_3@rGO with rhombohedral crystalline phase. It should be mentioned beforehand that the reported capacity values of V_2O_3 differ significantly in literature, depending on structure, morphology and modification with carbon. For example, V_2O_3-rGO has been reported to deliver first discharge capacity of 1400 mAh g^{-1} in the potential window of 0–3 V (*vs.* Li^+/Li) at 70 mA g^{-1}, with reversible capacity of 830 mAh g^{-1}.[6] Only 80 mAh g^{-1} was obtained by V_2O_3 nanorods in the same potential window at 100 mA g^{-1}.[31] Furthermore, as mentioned in the introductory part, Hong and co-workers calculated the Li storage capacity of V_2O_3 being as high as 1073 mAh g^{-1}, when considering the heterogeneous reaction of V_2O_3 being reduced to V° and the formation of V/Li_2O nanocomposites phases. However, the practical full Li uptake could not be attained.[19]

Following the developed rationale for V_2O_5 and VO_2 electrodes, we started by testing the electrochemical activity of V_2O_3@rGO in various potential windows. The results were unexpectedly different from V_2O_5 and VO_2 counterparts. First, when cycled in the potential window of 2.0–4.1 V (*vs.* Li^+/Li) at low current density of 10 mA g^{-1}, a very low capacity of 38 mAh g^{-1}_{V2O3} was attained (Figure 5). Complementary measurements on pure rGO electrodes (Figure S6) show that this capacity originates mainly from the capacitive charge storage at V_2O_3@rGO surface, with thus little contribution from redox of V_2O_3 in this potential window. This corroborates with the findings on V_2O_5 and VO_2 electrodes since the oxidation states attained, even when deep-cycled, were still above V^{3+}, signifying that further reduction of V_2O_3 would take place at lower potentials.

When extending the redox potential window down to 0.1 V (*vs.* Li^+/Li), an irreversible high capacity of 1189 mAh g^{-1}_{V2O3} was attained, with only 291 mAh g^{-1}_{V2O3} reversible (Figure 5). The subsequent re-charge sloping potential profile is also featureless. This can be first attributed to excessive decom-

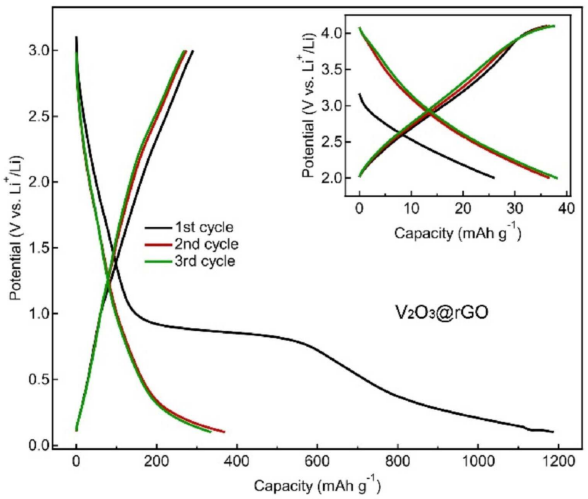

Figure 5. Galvanostatic charge-discharge profiles for V_2O_3@rGO electrode in potential window of 0.1–3.0 V (*vs.* Li^+/Li) at 10 mA $g^{-1}_{(V2O3)}$. Inset shows the 2.0–4.1 V region with stored charge attributed to combined capacitive charge storage of rGO and V_2O_3 nanocomposite.

position of the electrolyte at 0.8 V with further decomposition owing to additional surface catalytic effect of V_2O_3.[32] In a control experiment, a pure rGO electrode was tested under similar conditions. The potential profiles of pure rGO possess similar features to those of V_2O_3@rGO electrode, with also rGO delivering higher capacity (3677 mAh g^{-1}_{rGO}, Figure S6d), indicating the large capacity contribution of rGO to V_2O_3@rGO electrode (approximately 1037 mAh g^{-1} considering rGO content in the composite). Still, the extra-capacity attained below 0.8 V, could be also assigned to electrochemical activity of V_2O_3 either via intercalation, insertion or conversion reactions. However, the activity is minor, in comparison to V_2O_5 and VO_2 composites (Figure S8).

In an attempt to understand the absence of electrochemical activity of the synthesized V_2O_3@rGO composite, we have prepared electrodes without rGO, by investigating the behaviour of V_2O_3(CM)/SP electrode (refer to Table S1 and Experimental Section for details). Slow galvanostatic cycling (10 mA g^{-1}_{V2O3}, 0.1–3.0 V *vs.* Li^+/Li) combined with ex-situ XRD was applied (Figure 6). The charge-discharge profile resembles the V_2O_3@rGO composite with the onset of electrolyte decomposition at 0.8 V and an extended discharge (reduction) capacity. The reversibility is poor, below 20%. The minor response around 2.4 V is attributed to partial V_2O_3 oxidation during handling, and correspondingly electrochemical activity.

The extended tail beyond the primary SEI formation region, below 0.6 V, could be still assigned to conversion or insertion reactions and this was probed via ex-situ XRD (Figure 6b). No phase change was observed after deep-lithiation and subsequent polarizing to 3 V. A conversion reaction can be thus certainly excluded as no new phases or products (such as metallic V^0, Li_2O or Li_xV-alloys) were detected. More intriguing however, is that no additional peaks, neither peak shift could be detected, with the XRD pattern being identical between the pristine-deeply discharged-re-charged electrodes. This implies that the rhombohedral-phase V_2O_3 synthesized and studied in this work is electrochemically inert. In other words, the electrochemical reduction of V^{3+} to lower valence states is hindered requiring further investigation to understand whether this peculiar behaviour is thermodynamically or kinetically limited.

With the electrochemical activity and stability conditions established, we further studied and compared the power-rate performances of the synthesized electrode materials with similar mass loading, cell assembly and test conditions (refer to Experimental Section for details). The results are summarized in Figure 7. All commercial powder based electrodes display poor

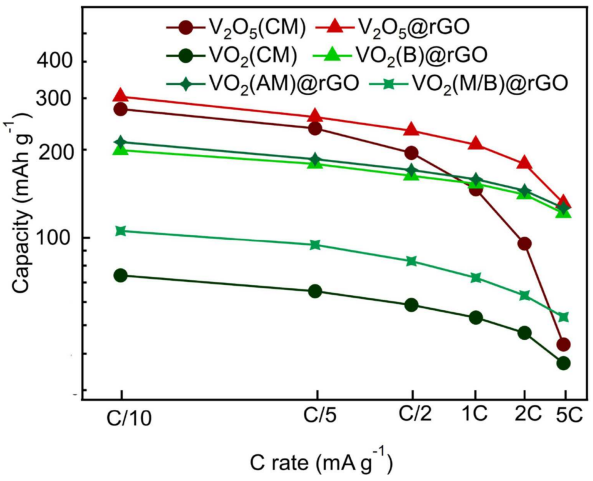

Figure 7. Rate capability of the V_2O_5 and VO_2 electrode materials in the potential window of 2.0–3.6 V (vs. Li^+/Li). (C = 100 mA $g^{-1}_{(VOx)}$)

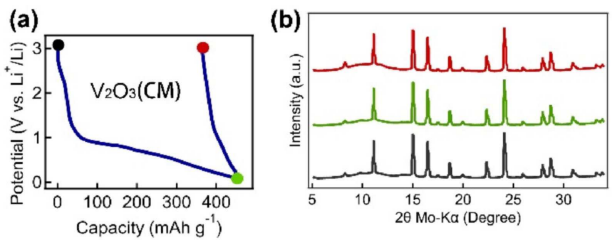

Figure 6. (a) Potential *vs.* specific capacity profiles for V_2O_3(CM)/SP in a potential window of 0.1–3.0 V (*vs.* Li^+/Li) at 10 mA $g^{-1}_{(V2O3)}$ and corresponding ex situ XRD patterns before cycling (black), after discharging to 0.1 V (green) and re-charging to 3.0 V (red).

rate performances. Of all, VO_2(CM) additionally shows poor material utilization even at low current density. In turn, V_2O_5 based electrodes all show high capacities at low rate and while the CM electrodes fail in delivering high power performances, the here synthesized V_2O_5@rGO shows best performances of all, with nearly 43% of the capacity (304 mAh g^{-1}_{V2O5}) retained at a current density of 500 mA g^{-1}_{V2O5} (equivalent of 5 C rate). Similar performance trends are found of VO_2@rGO composites. The results also show that (B) and (AM) phases of VO_2@rGO outperform V_2O_5@rGO in terms of capacity retention with applied current density. Whereas the low rate capacity for V_2O_5

is higher, VO_2 electrodes display better capacity retention: 61% for VO_2(B)@rGO and 59% for VO_2(AM)@rGO at 5 C rate. The amorphous VO_2@rGO electrode is competitive in rate capability but not superior to VO_2(B)@rGO phase counterpart, indicating power-rate performance is affected by nanostructuration and rGO charge transporter rather than phase kinetics. The general behaviour of the presented power-rate performances can be clearly explained by the fact that the Li^+ and electron transport distances are significantly shortened in the synthesized rGO nanocomposites, resulting in improved electrode kinetics and charge transfer.

Lastly, Na-ion storage properties have also been evaluated and the main results summarized in Figure 8. The electrochemical behaviour for Na storage was found to differ significantly as compared to Li storage. It can first be observed that all synthesized and analysed phases (V_2O_5@rGO, VO_2(B)@rGO and VO_2(AM)@rGO) have sloped potential-capacity profiles. The absence of noticeable potential plateau in the profiles of VO_2(B)@rGO could indicate the difficulty of Na^+ insertion into the crystalline VO_2(B). This can also explain lower Na storage capacities and higher electrode polarization (hysteresis). In turn, the V_2O_5@rGO with poor crystallinity and the amorphous VO_2(AM)@rGO can deliver comparable initial capacities to those of Li cells. Over 50 cycles, there is slight capacity loss for all electrodes, but retained capacities are still higher than those of bulk commercial electrode materials when tested in Na cells (Figure S9). The poor rate capability and deficient Na storage capacity for commercial counterparts reflect the positive effect of nanostructuring with rGO scaffold on electrochemical performance of the vanadium oxides.

Besides charge storage via guest species intercalation into ordered, crystalline structure of electrode materials, there exist capacitive storage mechanisms contributing to the overall charge storage capacity simultaneously. The later ones mostly can be reflected by sloping feature of potential profiles. It has been reported that the capacitive contribution of VO_2(B) electrode in Na cells plays the dominant role in the charge storage process, accounting for 76% of the total storage capacity.[10] In some previous studies, VO_x electrodes have been also found to exhibit potential profiles without noticeable plateaus and suffer from fast capacity decay.[29a,33] This could be attributed to larger size of Na^+ than Li^+ resulting in sluggish electrochemical reaction and gradual structure collapse during Na^+ insertion / extraction processes for electrode materials.

Amorphous materials have been considered as promising electrode candidates for alkali storage, because more open framework arising from disordered arrangement of atoms could potentially facilitate ionic diffusion. As shown above, VO_2(AM)@rGO shows similar Li storage performance to VO_2(B)@rGO, in terms of capacity values and rate capability (Figure 3). However, the amorphous phase outperforms the crystalline one when applied for Na storage. This indicates that amorphous electrode materials could be competitive to accommodate Na^+ and other alkali ions with larger ionic radius.

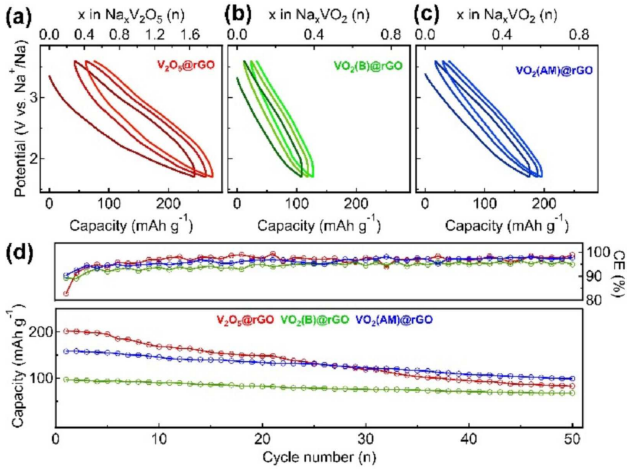

Figure 8. Sodium storage performances of V_2O_5@rGO and VO_2@rGO composite electrodes cycled at a current density of 10 mA g^{-1} $_{(VOx)}$. Potential *vs.* specific capacity and Na content profiles for (a) V_2O_5@rGO, (b) VO_2(B)@rGO and (c) VO_2(AM)@rGO in a potential window of 1.7–3.6 V (*vs.* Na^+/Na), and (d) cycling performance.

3. Conclusions

We developed a cost-effective, versatile and environmentally friendly synthetic approach for the decoration of rGO carbon with various VO_x nanostructures. The synthesis proceeds through green methods, relies on easily available precursors, gives high yield and limited waste generation thus making the methods proposed suitable for large-scale applications. This allowed us to synthesize a rich library of VO_x@rGO electrode materials making possible a systematic and critical comparison of their electrochemical performances. Both Li and Na ion storage properties were analysed.

Whereas precise quantitative guidelines will be dependent on specific composition, morphology and electrode formulation, the important findings of this work, that could be further generalized to other VO_x battery electrode composites, are: (i) the limited potential window for high capacity retention and coulombic efficiency. A balance needs to be found between the amount of stored charge and stable cycling; (ii) V_2O_5 can deliver more charge storage, while (B) and (AM) VO_2 phases are better choices as highly reversible and cycling stable cathodes; (iii) Power performances essentially depend on nanostructuration as well as carbon content and interfacing, while being minimally affected by the VO_x composition and crystal phase; (iv) Amorphous VO_x phases are more suitable for Na-ion storage, worthy of further investigation and optimisation; (v) Electrochemical reduction of V^{3+} seems to be unfavourable in solid-phase.

Overall, this work gives an exhaustive experimental overview on the electrochemistry of vanadium oxides composites and may be used as a baseline for future developments for this class of next-generation battery materials.

Experimental Section

Impregnation Synthesis of V_2O_5@rGO

The precursor solution was prepared by mixing V_2O_5 (91.5 mg, 99.9%, Alfa Aesar) and citric acid monohydrate (644 mg, GR for analysis, Merck) in 3.5 mL of Milli-Q water under vigorous stirring at 70 °C for 30 min (until the colour of the solution changed from yellow (V^{5+}) to blue (V^{4+})). rGO (35 mg, Graphene N002-PDR, Angstron Materials) was deposited into a crucible and impregnated with the solution to which 0.5 mL of methanol was added to improve wettability. After vacuum drying at 50 °C for 15 min, the powder was heated to 600 °C for one hour under Ar atmosphere. V_2O_5@rGO was finally obtained by heating the powders at 300 °C for 15 min in air.

Hydrothermal Synthesis of VO_2(B)@rGO

VO_2(B)@rGO was synthesized using hydrothermal conditions with oxalic acid, as previously reported.[34] In a typical synthesis, 35 mg of rGO was first dispersed in 35 mL Milli-Q water under sonication for 45 min. To increase the dispersibility of the hydrophobic rGO in water, 2 mL of methanol was added to the suspension. V_2O_5 (93.5 mg) and oxalic acid dihydrate (196 mg, GR for analysis, Merck) were added to the suspension, followed by stirring at 70 °C for 45 min, until the V_2O_5 was completely dissolved. Next, the mixture was poured into a 300 mL Teflon lined stainless steel autoclave and kept at 200 °C for 15 h while stirred at 200 rpm in a heating mantle. Finally, the product was vacuum-filtered through a 0.22 μm PVDF membrane and washed thoroughly with Milli-Q water and ethanol. VO_2(B)@rGO was obtained after drying under vacuum at 50 °C for 24 h.

Hydrothermal Synthesis of VO_2(AM)@rGO and V_2O_3@rGO

VO_2(AM)@rGO was obtained using the same protocol as VO_2(B)@rGO, except that the oxalic acid dihydrate was replaced by citric acid monohydrate (314 mg). V_2O_3@rGO was obtained by annealing VO_2(AM)@rGO at 500 °C for 2 h under reducing Ar/H_2 (5%) atmosphere. If annealed under non-reducing, pure Ar atmosphere, the VO_2(AM)@rGO became crystalline, denoted hereafter as VO_2(M/B)@rGO.

Materials Characterization

Thermogravimetric analysis (TGA) was performed with air as carrier gas, up to 900 °C, at a heating rate of 10 °C min^{-1} on a Mettler Toledo TGA/DSC 3$^+$ STAR^e System, using alumina containers. Powder X-ray diffraction (XRD) was employed to confirm the crystalline phases of the synthesized composite samples and compared to those of commercial materials: V_2O_5 (99.9%, Alfa Aesar), VO_2 (≥ 99%, Sigma-Aldrich) and V_2O_3 (98%, Sigma-Aldrich). The powders were introduced into 0.5 mm thin-walled glass capillaries (Hilgenberg GmbH, Germany), mounted on a goniometer head and kept at 200 mm distance from the detector. Diffractograms were collected at room temperature using a MAR345 diffractometer (MarResearch GmbH), a Mo–Kα (0.71073 Å) anode and a XENOCS focusing mirror. The obtained 2D diffractograms were azimuthally integrated using the Fit2D software and calibrated with a LaB_6 standard (NIST 660b Standard). The microstructure and morphology of the samples were characterized by Scanning Electron Microscopy (SEM, JEOL JSM 7600F), Energy-dispersive X-ray spectroscopy (EDX, JEOL JSM 7600F) and Transmission Electron Microscope (TEM, LEO 922 OMEGA) after dispersing these on holey carbon film on copper grids.

Electrochemical Measurements

The working electrodes were fabricated by dry grinding the VO_x@rGO composites (90 wt%) with Poly tetra fluoroethylene (PTFE, powder, Sigma-Aldrich) as binder (10 wt%), followed by pressing certain amount of powder onto coin cell case. The typical mass loading was of approximately 2–2.5 mg composite powder per square-cm. The commercial VO_x samples, denoted hereafter as VO_x(CM), were ball milled with super P carbon (SP) as conductive agent at 300 rpm for 2 h under Ar, followed by dry grinding with PTFE binder. For comparison purposes, the carbon content (approximately 30 wt.%) was kept similar to the VO_x@rGO counterparts, as listed in Table S1. Besides, rGO electrodes were also prepared by grinding with PTFE (27.6 wt.%).

The electrochemical characterization was performed in half-cells (CR2032 coin cell format) with either metallic Li or Na as counter and reference electrode and one sheet of glassfibre (Whatman, GF/D) separator. The assembly was performed in an Ar filled glove box (less than 0.1 ppm in water and oxygen). For Li half-cells, the electrolyte solution was made by dissolving 1 M $LiPF_6$ in a 1:1 (v:v) mixture of ethylene carbonate (EC) and dimethyl carbonate (DMC). Galvanostatic charge-discharge tests were carried out with various current densities and potential window conditions using Neware battery test system at ambient temperature. For Na half-cells, $NaClO_4$ dissolved in a 1:1 (v:v) mixture of EC and diethyl carbonate (DEC) containing 5 vol% fluoroethylene carbonate (FEC) was used. Galvanostatic charge-discharge tests were performed for Na cells on Neware battery testing system at ambient temperature. Reported capacities are per gram of VO_x in the electrodes, denoted as mAh g$^{-1}_{(VOx)}$.

Ex Situ XRD Measurement

To confirm the electrochemical inactivity of the synthesized V_2O_3 composite, the cells containing commercial V_2O_3, were first discharged to 0.1 V (vs. Li^+/Li) or subsequently re-charged to 3.0 V (vs. Li^+/Li) at a current density of 10 mA g$^{-1}_{(V2O3)}$. Subsequently, the cells were disassembled in the glovebox, and the electrode powder was collected and then washed with DMC. After drying, the powder was sealed in glass capillaries for XRD analysis.

Acknowledgements

X. L. acknowledges China Scholarship Council for financial support. This work was funded by CF-ARC (18/23-093) MICROBAT and NANO4WAVES grants. Funding was also received through F. R.S. FNRS T.009913F grant.

Conflict of Interest

The authors declare no conflict of interest.

Keywords: energy storage · hydrothermal synthesis · lithium storage · sodium storage · vanadium oxide

[1] M. O. Guerrero-Pérez, *Catal. Today* **2017**, *285*, 226–233.
[2] J. Huotari, R. Bjorklund, J. Lappalainen, A. Lloyd Spetz, *Sens. Actuators B* **2015**, *217*, 22–29.
[3] P. Liu, K. Zhu, Y. Gao, H. Luo, L. Lu, *Adv. Energy Mater.* **2017**, *7*.

[4] a) N. Nitta, F. Wu, J. T. Lee, G. Yushin, *Mater. Today* **2015**, *18*, 252–264; b) H. Li, P. He, Y. Wang, E. Hosono, H. Zhou, *J. Mater. Chem.* **2011**, *21*; c) N. A. Chernova, M. Roppolo, A. C. Dillon, M. S. Whittingham, *J. Mater. Chem.* **2009**, *19*; d) Y.-B. Kang, *J. Eur. Ceram. Soc.* **2012**, *32*, 3187–3198; e) H. Zhao, L. Pan, S. Xing, J. Luo, J. Xu, *J. Power Sources* **2013**, *222*, 21–31.
[5] a) M. Liu, B. Su, Y. Tang, X. Jiang, A. Yu, *Adv. Energy Mater.* **2017**, *7*; b) J. Yao, Y. Li, R. C. Massé, E. Uchaker, G. Cao, *Energy Storage Mater.* **2018**, *11*, 205–259.
[6] J. Leng, H. Mei, L. Zhan, Y. Wang, S. Yang, Y. Song, *Electrochim. Acta* **2017**, *231*, 732–738.
[7] A. S. Aricò, P. Bruce, B. Scrosati, J.-M. Tarascon, W. V. Schalkwijk, *Nat. Mater.* **2005**, *4*, 366–377.
[8] a) G. Wang, X. Shen, J. Yao, J. Park, *Carbon* **2009**, *47*, 2049–2053; b) M. J. Allen, V. C. Tung, R. B. Kaner, *Chem. Rev.* **2010**, *110*, 132–145.
[9] Y. Yang, L. Li, H. Fei, Z. Peng, G. Ruan, J. M. Tour, *ACS Appl. Mater. Interfaces* **2014**, *6*, 9590–9594.
[10] N. B. Mahadi, J.-S. Park, J.-H. Park, K. Y. Chung, S. Y. Yi, Y.-K. Sun, S.-T. Myung, *J. Power Sources* **2016**, *326*, 522–532.
[11] B. Xiao, B. Zhang, L.-B. Tang, C.-S. An, Z.-j. He, H. Tong, W.-J. Yu, J.-C. Zheng, *Ceram. Int.* **2018**, *44*, 15044–15049.
[12] C. Delmas, C.-A. H. J. M. Cocciantelli, M. Ménétrier, J. P. Doumerc, *Solid State Ionics* **1994**, *69*, 257–264.
[13] a) H. Liu, W. Yang, *Energy Environ. Sci.* **2011**, *4*, 4000–4008; b) M. S. Whittingham, *Chem. Rev.* **2004**, *104*, 4271–4302.
[14] C. K. Chan, H. Peng, R. D. Twesten, K. Jarausch, X. F. Zhang, Y. Cui, *Nano Lett.* **2007**, *7*, 490–495.
[15] C. K. Christensen, D. R. Sørensen, J. Hvam, D. B. Ravnsbæk, *Chem. Mater.* **2018**, *31*, 512–520.
[16] a) O. B. Chae, J. Kim, I. Park, H. Jeong, J. H. Ku, J. H. Ryu, K. Kang, S. M. Oh, *Chem. Mater.* **2014**, *26*, 5874–5881; b) F. Mattelaer, K. Geryl, G. Rampelberg, J. Dendooven, C. Detavernier, *ACS Appl. Mater. Interfaces* **2017**, *9*, 13121–13131.
[17] a) C. Leroux, G. Nihoul, G. V. Tendeloo, *Phys. Rev. B* **1998**, *57*, 5111–5121; b) T. Chirayil, P. Y. Zavalij, M. S. Whittingham, *Chem. Mater.* **1998**, *10*, 2629–2640; c) H. J. Song, M. Choi, J. C. Kim, S. Park, C. W. Lee, S. H. Hong, B. K. Kim, D. W. Kim, *Sci. Rep.* **2016**, *6*, 30202; d) Y. Chen, S. Zhang, F. Ke, C. Ko, S. Lee, K. Liu, B. Chen, J. W. Ager, R. Jeanloz, V. Eyert, J. Wu, *Nano Lett.* **2017**, *17*, 2512–2516.
[18] a) L. Liu, Q. Liu, W. Zhao, G. Li, L. Wang, W. Shi, L. Chen, *Nanotechnology* **2017**, *28*, 065404; b) L. Mai, Q. Wei, Q. An, X. Tian, Y. Zhao, X. Xu, L. Xu, L. Chang, Q. Zhang, *Adv. Mater.* **2013**, *25*, 2969–2973; c) P. Liu, Y. Xu, K. Zhu, K. Bian, J. Wang, X. Sun, Y. Gao, H. Luo, L. Lu, J. Liu, *J. Mater. Chem. A* **2017**, *5*, 8307–8316; d) S. Wang, K. A. Owusu, L. Mai, Y. Ke, Y. Zhou, P. Hu, S. Magdassi, Y. Long, *Appl. Energy* **2018**, *211*, 200–217.
[19] H. Lia, P. Balaya, J. Maier, *J. Electrochem. Soc.* **2004**, *151*, A1878–A1885.
[20] a) M. Clites, E. Pomerantseva, *Energy Storage Mater.* **2018**, *11*, 30–37; b) H. D. Yoo, J. R. Jokisaari, Y.-S. Yu, B. J. Kwon, L. Hu, S. Kim, S.-D. Han, M. Lopez, S. H. Lapidus, G. M. Nolis, B. J. Ingram, I. Bolotin, S. Ahmed, R. F. Klie, J. T. Vaughey, T. T. Fister, J. Cabana, *ACS Energy Lett.* **2019**, 1528–1534; c) W. Luo, J.-J. Gaumet, L. Mai, *MRS Commun.* **2017**, *7*, 152–165.
[21] X. Liu, J. Zeng, H. Yang, K. Zhou, D. Pan, *RSC Adv.* **2018**, *8*, 4014–4031.
[22] S. Park, J. An, J. R. Potts, A. Velamakanni, S. Murali, R. S. Ruoff, *Carbon* **2011**, *49*, 3019–3023.
[23] A. Van der Ven, J. Bhattacharya, A. A. Belak, *Acc. Chem. Res.* **2013**, *46*, 1216–1225.
[24] a) Y. Dou, X. Liang, G. Gao, G. Wu, *J. Alloys Compd.* **2018**, *735*, 109–116; b) X. Liang, G. Gao, G. Wu, H. Yang, *Electrochim. Acta* **2016**, *188*, 625–635; c) Z. Cao, B. Wei, *Nano Energy* **2013**, *2*, 481–490.
[25] a) C. Leger, S. Bach, P. Soudan, J. P. Pereira-Ramos, *J. Electrochem. Soc.* **2005**, *152*; b) D. Aurbach, B. Markovsky, G. Salitra, E. Markevich, Y. Talyossef, M. Koltypin, L. Nazar, B. Ellis, D. Kovacheva, *J. Power Sources* **2007**, *165*, 491–499.
[26] Y. Yue, H. Liang, *Adv. Energy Mater.* **2017**, *7*.
[27] P. Arora, R. E. White, M. Doyle, *J. Electrochem. Soc.* **1998**, *145*, 3647–3667.
[28] A. Van der Ven, J. Bhattacharya, A. A. Belak, *Acc. Chem. Res.* **2013**, *46*, 1216–1225.
[29] a) E. Uchaker, Y. Z. Zheng, S. Li, S. L. Candelaria, S. Hu, G. Z. Cao, *J. Mater. Chem. A* **2014**, *2*, 18208–18214; b) H. Si, L. Seidl, E. M. L. Chu, S. Martens, J. Ma, X. Qiu, U. Stimming, O. Schneider, *J. Electrochem. Soc.* **2018**, *165*, A2709–A2717.
[30] a) D. Chao, C. Zhu, X. Xia, J. Liu, X. Zhang, J. Wang, P. Liang, J. Lin, H. Zhang, Z. X. Shen, H. J. Fan, *Nano Lett.* **2015**, *15*, 565–573; b) Q. Zhao, L. Jiao, W. Peng, H. Gao, J. Yang, Q. Wang, H. Du, L. Li, Z. Qi, Y. Si, Y. Wang, H. Yuan, *J. Power Sources* **2012**, *199*, 350–354.
[31] X. Li, J. Fu, Z. Pan, J. Su, J. Xu, B. Gao, X. Peng, L. Wang, X. Zhang, P. K. Chu, *J. of Power Sources* **2016**, *331*, 58–66.
[32] A. Ponrouch, P.-L. Taberna, P. Simon, M. R. Palacín, *Electrochim. Acta* **2012**, *61*, 13–18.
[33] a) H. Wang, X. Gao, J. Feng, S. Xiong, *Electrochim. Acta* **2015**, *182*, 769–774; b) D. W. Su, S. X. Dou, G. X. Wang, *J. Mater. Chem. A* **2014**, *2*.
[34] G. He, L. Li, A. Manthiram, *J. Mater. Chem. A* **2015**, *3*, 14750–14758

Manuscript received: August 18, 2019
Accepted manuscript online: August 22, 2019
Version of record online: September 11, 2019